Highly sensitive terahertz thin film total internal reflection spectroscopy reveals in situ photo-induced structural changes in methylammonium lead halide perovskites

Qiushuo Sun[†‡], Xudong Liu[†‡], Jie Cao[†], Rayko I. Stantchev[†], Yang Zhou[†], Xuequan Chen[†], Edward P. J. Parrott[†], James Lloyd-Hughes[§], Ni Zhao[†] and Emma Pickwell- MacPherson[†§]*

[†] Department of Electronic Engineering, The Chinese University of Hong Kong, Hong Kong

[§] Department of Physics, University of Warwick, Gibbet Hill Road, Coventry, CV4 7AL, United Kingdom

[‡] The first two authors have contributed equally to this work.

[*] Corresponding author, e.pickwell.97@cantab.net

KEYWORDS: Perovskites, photo-induced structural changes, terahertz total internal reflection spectroscopy.

ABSTRACT

THz thin film total internal reflection (TF-TIR) spectroscopy is shown to have an enhanced sensitivity to the vibrational properties of thin films in comparison to standard THz transmission spectroscopy. This increased sensitivity was used to track photo-induced modifications to the structure of thin films of methylammonium (MA) lead halide, $MAPbI_{3-x}Br_x$ (x=0, 0.5, 1, 3). Initially, illumination strengthened the phonon modes around 2THz, associated with Pb-I stretch modes coupled to the MA ions, while the 1THz twist modes of the inorganic octahedra did not alter in strength. Under longer term illumination the 1THz phonon modes of encapsulated films slowly reduced in strength, while in films exposed to moisture and oxygen these phonons weaken more rapidly and blueshift in frequency. The rapid monitoring of environmentally-induced changes to the vibrational modes afforded by TF-TIR spectroscopy offers applications in the characterization and quality control of perovskite thin-film solar cells and other thin-film semiconductors.

TABLE OF CONTENTS IMAGE

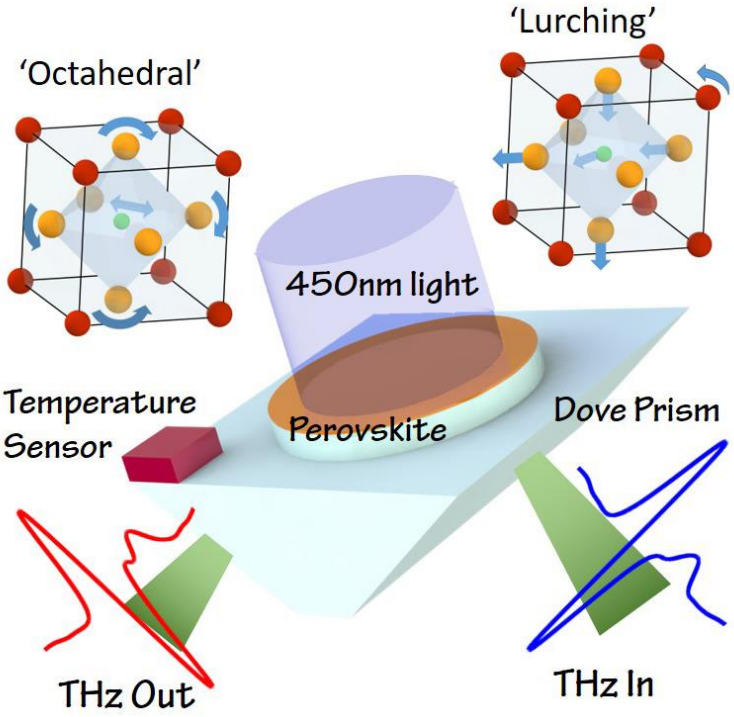

The rapid development of organic-inorganic halide perovskite materials has facilitated their use in photovoltaic solar cells (PSCs)[1-3], LEDs[4] and lasers[5]. However, concerns about the stability of halide perovskites have been raised as a major issue that obstructs their practical applications: water, oxygen, light and heat can cause halide perovskites to degrade.[1-2] The degradation of perovskites can be slowed down by proper encapsulation or by partially replacing MA with formamidinium (FA).[1]

Above bandgap illumination can alter the structural and functional electronic properties of halide perovskites, even while remaining within the perovskite phase. In MA perovskites photo-induced carriers reduce the binding energy and increase the rotational freedom of the MA cation[6], inducing a giant dielectric response[7]. UV illumination was found to alter the Raman lines and photoluminescence intensity of $MAPbI_3$ reversibly, attributed to changes in the inorganic octahedra to adapt to light-induced rotations in the MA cations.[8-9] In mixed halide perovskites, where the bandgap can be tuned via the iodine to bromine ratio,[10] light can stimulate the halide ions to segregate into Br-rich and I-rich domains with different band-gaps[11-12].

Common vibrational spectroscopy methods such as Raman, Fourier Transform Infrared Spectroscopy and terahertz (THz) time-domain spectroscopy have been widely utilized to study the vibrational modes of the perovskite crystalline lattice, and the organic cation[13-16]. THz time-domain spectroscopy in particular is attractive, as it probes the low-frequency vibrational modes that dominate the electron-phonon scattering rate, and thus the room temperature mobility[13, 17]. Previously, THz-TDS was used to study the vibrational modes in the orthorhombic, tetragonal and cubic phases of $MAPbX_3$ perovskites[16-17], and to investigate the kinetics of $MAPbI_3$ crystal formation from precursors during annealing[18]. In these experiments standard THz-TDS transmission setups were utilized, typically yielding less than 10% amplitude change between sample and reference measurements for typical film

thicknesses.[16] In order to obtain sufficiently precise spectrally-resolved data, long integration times (>10 minutes) are often needed, restricting the usefulness of THz-TDS transmission spectroscopy to monitor environmentally-induced changes in the vibrational modes of perovskite thin films on shorter timescales.

In this Letter, we report that THz thin film total internal reflection (TF-TIR) spectroscopy is a sensitive probe of the vibrational modes of perovskite thin films, and validate the high sensitivity of this method. Utilizing this advance, we studied light-induced modifications to the vibrational modes of single and mixed halide $MAPbX_3$. Time-dependent changes in the vibrational mode strength, frequency and linewidth were tracked under different environmental conditions. A thin film encapsulation layer, made of poly(perfluorobutenylvinylether) (CYTOP), was optionally used to mitigate against the effects of exposure to moisture and oxygen. Complementary X-ray diffraction (XRD) and photoluminescence (PL) measurements of the perovskite thin film samples under the same environmental conditions were used to monitor the structure and band edge emission.

Enhanced THz responsivity by TF-TIR. The THz time domain signals of a pristine $MAPbI_3$ perovskite sample measured in transmission and in the TF-TIR geometry are shown in Figure 1 (a-b). In transmission the THz pulse amplitude reduced by 5.4% in comparison to the reference substrate, while in the TF-TIR geometry the signal change was larger, at 9.1%. The higher sensitivity of the TIR geometry to the conductivity of thin films in comparison to the transmission method has been previously established for graphene,[19-21] and is expanded upon below.

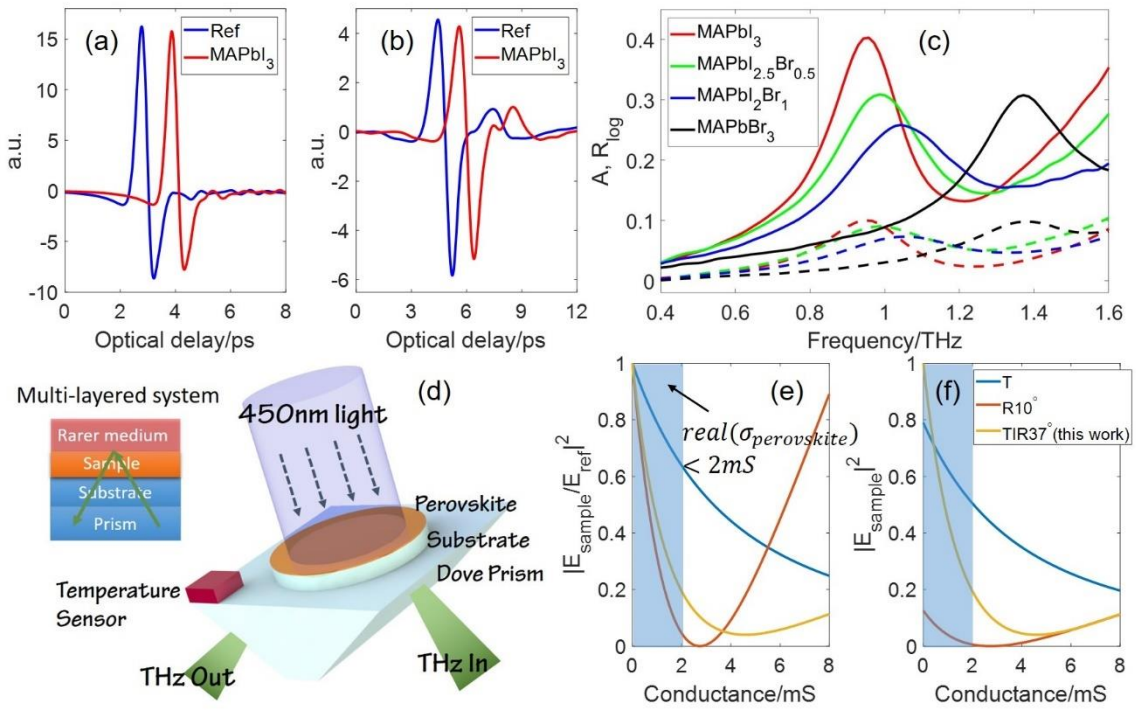

Figure 1. THz time domain signals of a $MAPbI_3$ perovskite sample and the bare substrate measured in the (a) Transmission system; (b) TF-TIR system. The sample signals are shifted horizontally for clarity. (c) The spectra of the pristine perovskite samples. Dashed lines were measured in transmission while solid lines were measured by TF-TIR. (d) Dove prism setup for THz TF-TIR and schematic of multi-layered system in this setup. Green arrows show the optical paths of the THz light. (e) Normalized and (f) absolute THz amplitudes as a function of sheet conductance calculated by Eqn (2), assuming the reference has a sample conductance of zero. 'T', 'R' and 'TIR' correspond to transmission, ordinary reflection and total internal reflection geometry.

The THz spectra for four samples of $MAPbX_3$ are shown in Figure 1 (c), as obtained from Eqns (1-2). The absorbance, A, was small (less than 0.1 for the four perovskite samples), which can be a challenge to measure accurately in lower signal-to-noise ratio systems. For the TF-TIR data we plot the logarithmic reflectance, $R_{\log}$ (see Methods), which was ~4 times

stronger (peaking at ~0.4) and matched the spectral shape of A. While the height of A and R_{log} depend on the thickness of the film, the data presented were obtained on the same films and thus offer a direct comparison between the performance of the different geometries.

For $MAPbI_3$ a clear peak is evident at 0.96 THz in both A and R_{log}, which can be assigned to I-Pb-I bond bending, creating distortions and twists of the inorganic octahedra[13], denoted here as the "octahedral" mode. The increased absorbance/reflectance at higher frequencies is created by a second set of vibrational modes around 2 THz, attributed to the stretching of the Pb-I bond coupled to MA cations[16, 22] referred to as the "lurching" mode[13]. These vibrational modes have been reported previously using transmission THz-TDS[16, 18, 22-23]. The observed increase in mode frequency (0.96, 0.99, 1.05 and 1.38 THz) with Br substitution is likely due to the lower average mass of the X site when Br replaces I[13]. However, the resonance frequency did not scale linearly with Br content: even with the bromine concentration increasing to 1/3, the resonant frequency only had a small blue shift and was still close to that of $MAPbI_3$, while there was an abrupt change to 1.38 THz for the pure bromine $MAPbBr_3$. This may be a result of the differing crystal system for pure $MAPbBr_3$ at room temperature, which is cubic with space group Pm3m, while $MAPbI_3$ is tetragonal with space group I4/mcm[13].

To provide insight into the enhanced sensitivity in the TF-TIR geometry, consider the schematic of the experimental geometry for TF-TIR shown in Figure 1(d). Here, the sample layer is a conductive thin film that is sandwiched by a rarer medium (lower refractive index, in this case air), and a substrate that is index-matched to the prism. The sample has an optical conductance σ_{sample} including contributions from both free charge motion and vibrational absorption. THz light penetrates the sample to the top interface with the rarer medium, as the sample thickness is smaller than the penetration depth. The reflection coefficient (s-polarized) of this three-phase system can be written as:[20]

$$r = \frac{n_{substrate}\cos\theta_{substrate} - n_{rarer}\cos\theta_{rarer} - Z_0\sigma_{sample}}{n_{substrate}\cos\theta_{substrate} + n_{rarer}\cos\theta_{rarer} + Z_0\sigma_{sample}} \quad (1)$$

where Z_0 is the impedance of vacuum and θ are the angles in the media. To compare the sensitivity of transmission, ordinary reflection (10°) and TIR geometry (37°), the THz response is given in Figure 1(e-f) as a function of σ_{sample}. The real part of σ_{sample} for $MAPbI_3$ peaks at 0.6mS at the phonon resonance around 1THz,[16] and hence the shaded range, Re $[\sigma_{sample}] < 2$mS, was representative of the vibrational modes of $MAPbX_3$. The slope marks the relative sensitivity: the ordinary reflection geometry (10°) has the best sensitivity, corresponding to the most rapid change in the measured $R_{\log}$ with changes to σ_{sample}, while the transmission geometry has the worst sensitivity. However, the least signal is collected in the ordinary reflection spectroscopy (Figure 1(f)), whilst TIR yields greater amplitude, improving the signal to noise ratio (SNR). The high sensitivity and SNR make THz TF-TIR geometry particularly suitable to characterize the vibrational phonon modes in perovskites during environmentally-driven changes.

Illumination alters the "lurching" vibrational modes. The THz spectra before, after 5 minutes of illumination and after resting in the dark for 5 minutes were measured with TF-TIR for encapsulated $MAPbI_3$, $MAPbI_{2.5}Br_{0.5}$, $MAPbI_2Br_1$ and $MAPbBr_3$, with the results shown in Figure 2. In all samples, short-term illumination increased the strength of the 'lurching' modes, evident from the increase in $R_{\log}$ at high frequencies, without changing the strength of the 'octahedral' modes. After resting in the dark for 5 minutes $R_{\log}$ recovered partially towards its shape before the light soaking, apart from the spectrum of $MAPbBr_3$, which overshot the original shape. Since our TF-TIR cannot measure above 1.7THz, a CYTOP encapsulated $MAPbI_{2.5}Br_{0.5}$ sample was measured in the transmission geometry on an alternative THz-TDS system with higher bandwidth (2.5THz), before illumination and after 5 minutes of rest in the dark after the 5 minutes illumination. The results (Figure S1)

show that the 'lurching' modes at 2 THz became stronger after 5 minutes rest in the dark after light soaking. Supplementary PL spectra following the same illumination protocol are reported in Figure S2. However, apart from strong phase segregation in $MAPbI_2Br_1$, PL spectra failed to reveal any effects of 5 minutes light soaking on the perovskites.

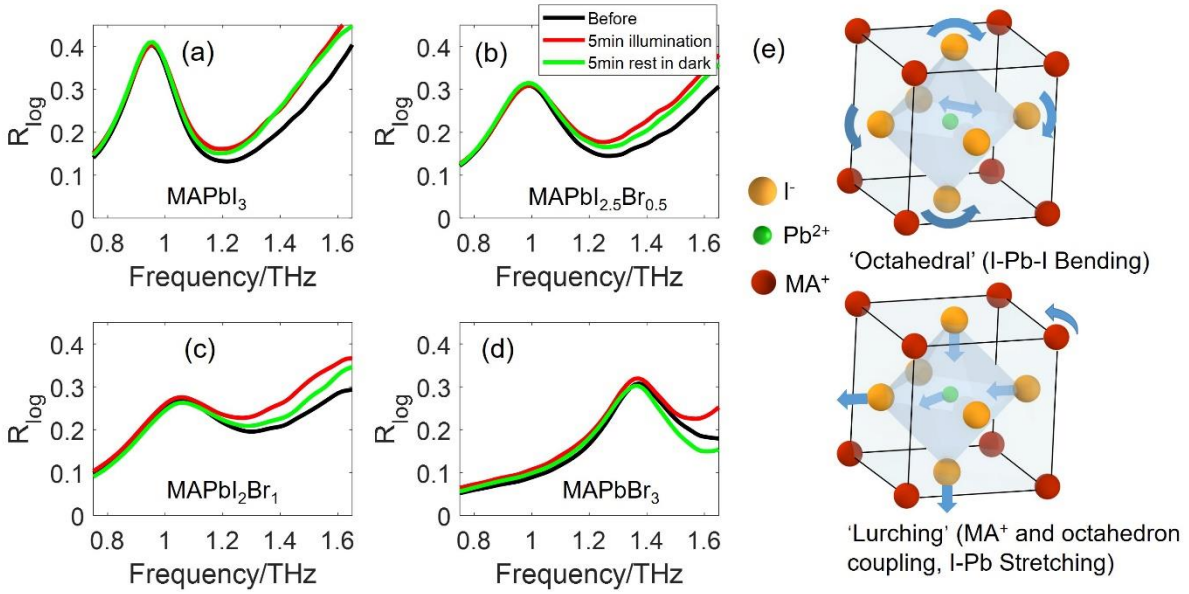

Figure 2. THz TF-TIR spectra before (black), after 5 minutes of illumination (red) and after 5 minutes rest in the dark (green) of CYTOP encapsulated (a) $MAPbI_3$, (b) $MAPbI_{2.5}Br_{0.5}$, (c) $MAPbI_2Br_1$ and (d) $MAPbBr_3$. (e) Crystal structure of $MAPbI_3$, showing the 'octahedral' and 'lurching' modes.

We now consider possible explanations for the change in the 'lurching' mode's strength. Phase segregation[11] cannot be the dominant cause, as it was observed for the two single halide perovskites. The combined effects of oxygen and light were ruled out by further tests on samples encapsulated in glass instead of CYTOP (since CYTOP has perfect isolation to moisture but not to oxygen[24]) reported in the Supplemental Information Figure S3. Partial decomposition of the perovskites was excluded using XRD spectra measured before and after 5 minutes of light soaking (Supplemental Figure S4). Having ruled out these other mechanisms we conclude that short-term illumination deforms the perovskite lattice.

Illumination can rotate MA cations and reduce their binding strength to the inorganic octahedra, as evidenced by DFT calculations[6] and experiment[8]. Consequently, we presume that after illumination the MA cations decreased its binding to the octahedra, enhancing the oscillator strength of the 'lurching' modes. When the light was switched off, this structural distortion recovered slowly, as the MA cations return to their original orientation and position.

Stability of encapsulated films under longer-term illumination. In contrast to the spectra after short-term illumination, where the 'lurching' modes strengthened and the 'octahedral' modes were unchanged, on longer timescales (up to 300min) both the 'octahedral' and 'lurching' absorption became moderately weaker, as reported in Figure 3 (a-d). Representative errorbars are given in Figure 3(a): the light induced spectral changes are very small even after 5 hours, improving the sensitivity by TF-TIR spectroscopy made it possible to track these subtle changes in oscillator strength. To further track these changes, the spectra were fitted by Lorentz Oscillator model (LOM, see METHOD section) with two Lorentzian oscillators, and the fitted frequency f_0, amplitude A and linewidth γ are shown in Figure 3(e-g) for the 'octahedral' mode, the details of LOM fitting can be found in Supplemental information. $MAPbI_2Br_1$ has the most significant (29%) drop in oscillator strength over 300 minutes, compared to 12%, 13% and 18% for $MAPbI_3$, $MAPbI_{2.5}Br_{0.5}$ and $MAPbBr_3$, respectively. The faster degradation speed of $MAPbI_2Br_1$ was likely caused by ion migration[25] in $MAPbI_2Br_1$ as there is a more severe lattice mismatch with increasing bromine concentration[11-12, 26]. The PL results in Figure S2 also confirmed this: the peak shift of $MAPbI_2Br_1$ is more significant than that of $MAPbI_{2.5}Br_{0.5}$ spectra.

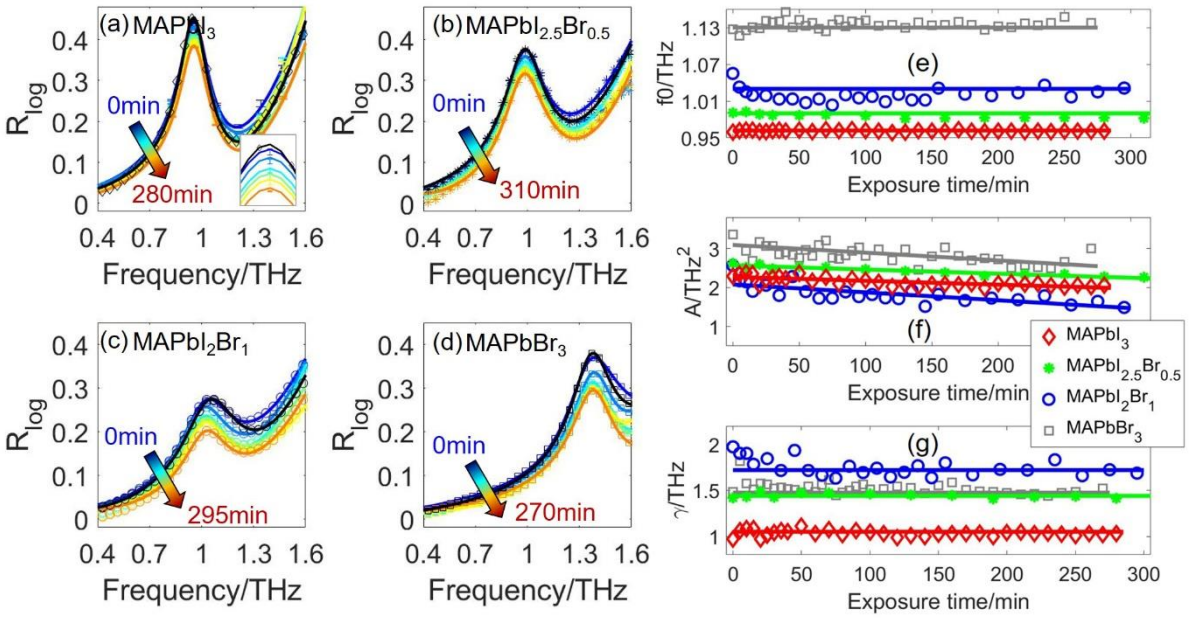

Figure 3. THz spectra from 0.4 THz to 1.6 THz of the CYTOP encapsulated (a) $MAPbI_3$ (b) $MAPbI_{2.5}Br_{0.5}$ (c) $MAPbI_2Br_1$ (d) $MAPbBr_3$ sample varying with exposure times. Representative errorbars are given in Figure 3(a): the inset highlights the error bars around the peak. Black color indicates the spectra before the illumination. Markers are measured data, curves are fits using two Lorentzian oscillators. Fitted (e) resonant frequencies, (f) strengths and spectral widths of the 'octahedral' peaks. The resonant frequencies of $MAPbBr_3$ in (e) were shifted vertically (minus 0.25 THz) for clarity.

To establish whether the LED illumination was the dominant cause of the long-term reduction in vibrational mode strength, a control group was stored in the dark under the same atmospheric conditions. The visual images, XRD pattern and THz TF-TIR spectra of a $MAPbI_2Br_1$ control sample after 300 minutes in the dark are presented in Figures 4 (a-c). The control exhibited no clear difference visually or in the THz spectra. The XRD peaks lowered in intensity slightly for the control sample, indicating a reduction in crystallinity irrespective of illumination. The sample illuminated for 300min had a more marked reduction in crystallinity, and broader peaks, resulting from a reduced crystallinity of the perovskite thin

film and a decreased grain size, respectively[27]. The reduction in strength of the THz vibrational modes is commensurate with the structural changes observed in XRD.

Furthermore, this photo-induced change was partially reversible, as evidenced in Figure 4 (d), for an encapsulated $MAPbI_2Br_1$ sample before, after 300 minutes illumination, and after recovery in the dark for 40 minutes. This reversible effect was observed for the three other compositions. The reversibility suggest that it was not the degradation into PbI_2 and $PbBr_2$ that caused the reduction of the peak strength[8].

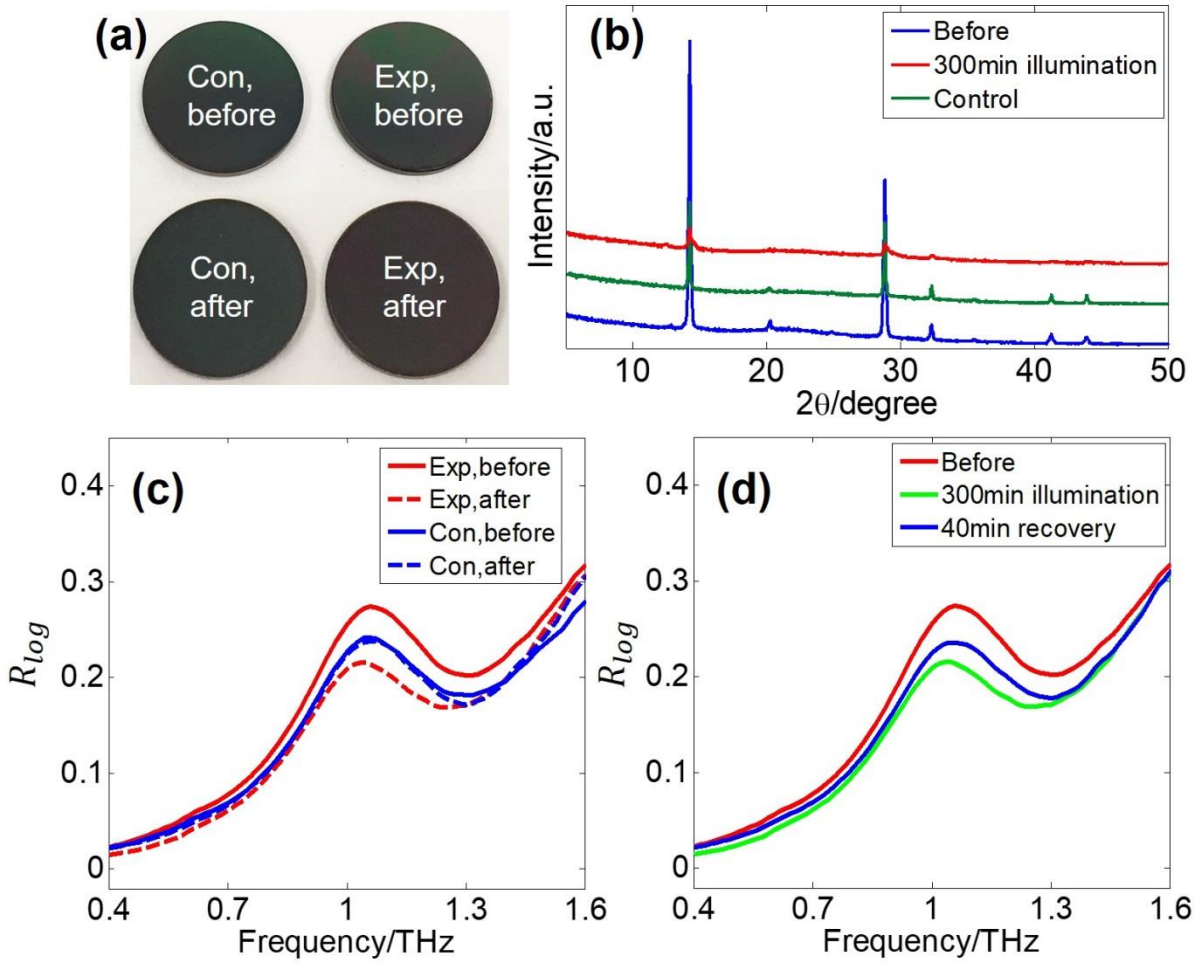

Figure 4. (a) visual images (b) XRD patterns (c) THz TF-TIR spectra of the encapsulated $MAPbI_2Br_1$ before, after 300 minutes illumination (experimental group), after 300 minutes being kept in dark (control group). The color of the sample turned brown slightly after 300 minutes of light soaking, which could be barely seen by the naked eye. (b) THz TF-TIR

spectra of the encapsulated $MAPbI_2Br_1$ before, after 300 minutes of illumination and after recovering for 40 minutes in dark.

Stability under moisture, oxygen and long-term illumination

To explore the effects of moisture and oxygen on the vibrational modes, we conducted measurements on perovskite thin films made without encapsulation. Figures 5 (a-d) show the photo-induced spectral changes in the perovskites during 0-280 minutes of illumination with exposure to moisture, oxygen, heat and light. In the presence of moisture, the perovskites were more sensitive to light and heat and were photo-modified much quicker than the encapsulated ones.

$MAPbI_3$ presented the fastest change: after 30 minutes, the 'octahedral' mode had totally disappeared. At this time little of the perovskite phase remains owing to its decomposition into PbI_2, MAI, CH_3NH_2, and I_2[28-29] as evidenced by visual inspection and XRD (Supplemental Figure S5). The control samples did not degrade: in fact $R_{log}$of the control was marginally enhanced by 30 minutes in the dark, as explained by exposure to humid air for short time[18]. This portrays the highly unstable nature of $MAPbI_3$ when exposed to moisture, oxygen and light. In contrast, for the two mixed halide perovskites, it took around 100 minutes before the phonon modes had vanished. After 110 minutes illumination there was no clear difference visually for $MAPbI_2Br_1$, and while the XRD intensity decreased, no PbI_2 peak had emerged (Supplemental Figure S5).

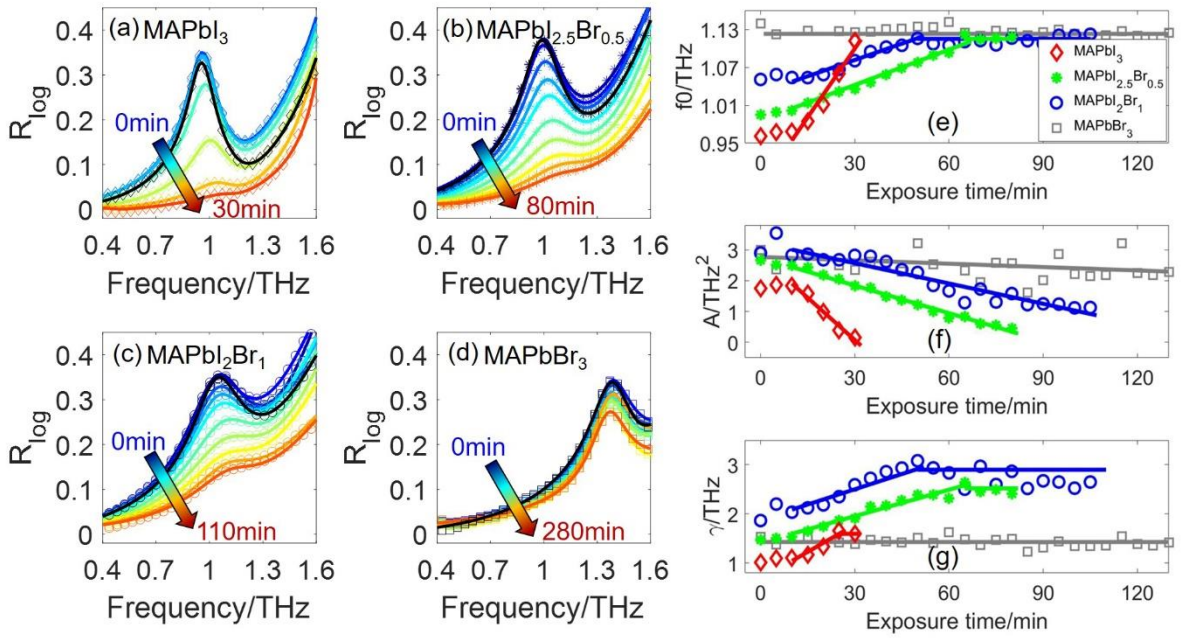

Figure 5. THz spectra from 0.4 THz to 1.6 THz of the non-encapsulated (a) $MAPbI_3$ (b) $MAPbI_{2.5}Br_{0.5}$ (c) $MAPbI_2Br_1$ (d) $MAPbBr_3$ sample varying with exposure times. Black color indicates the spectra before the illumination. Dots are measured data, curves are the two-oscillator Lorentzian fits. Fitted (e) resonant frequencies, (f) strengths and (g) spectral widths of the 'octahedral' peak over 120 minutes of illumination. The resonant frequencies of $MAPbBr_3$ in (e) were shifted vertically (minus 0.25 THz) for clarity.

The spectra were fitted using the same model as above, yielding the parameters given in Figures 5 (e-g). During illumination, a subtle blue shift of the lowest vibrational mode with time was observed, apart from $MAPbBr_3$ where the oscillator strength reduced marginally. For $MAPbI_3$, $MAPbI_{2.5}Br_{0.5}$ and $MAPbI_2Br_1$, over the 30/80/110 minutes of the illumination, the resonant frequencies of the spectral peaks shifted from 0.96, 0.99 and 1.05 THz to around 1.11 THz (frequency shifts 0.15, 0.12 and 0.06 THz, respectively). This blueshift with time may result from the light-induced formation of iodide vacancies, which would lower the average mass and increase the frequency of the Pb-I buckling modes. The Pb-I bond is fragile

in comparison to Pb-Br:[29] the decomposition energy in $MAPbI_3$ is as low as 0.1 eV[30]. The spectral widths similarly increased with time due to the increased structural disorder.

The huge difference in deterioration rate between the encapsulated (Figure 3) and non-encapsulated (Figure 5) $MAPbI_3$ samples demonstrates that moisture accelerates the breakdown of the structure, whereas the rate for $MAPbBr_3$ was comparable with and without encapsulation. The better stability of Br compound in the presence of moisture is explained by reduced lattice constant and the transition to cubic phase, which is more stable than tetragonal phase [31].

Herein we demonstrated for the first time that THz TF-TIR spectroscopy is a sensitive method to study the vibrational modes of thin films of lead-halide perovskites. The increased sensitivity afforded by the TIR geometry allowed subtle changes in the vibrational modes associated with the inorganic octahedra and coupled Pb-X-MA modes to be explored in different environmental conditions and in-situ under illumination. From the experimental results, we deduce there was a two-step structural change in the perovskite thin films under illumination: firstly the intensity of the 'lurching' modes was enhanced after 5 minutes of illumination; secondly long-term light soaking induced a decrease in the intensity of both 'octahedral' and 'lurching 'phonon modes, and the 'octahedral' modes had a blue shift in the presence of moisture. Our results give direct experimental evidence for the hypothesis proposed by Gottesman *et al.*[8]: inorganic octahedra realign to adapt to the rotated MA cations induced by illumination. A thorough knowledge of the vibrational modes is increasingly identified as important because the LO-phonon modes are thought to control the room temperature charge mobility [16, 32]. THz TF-TIR provides a novel way to study the stability of perovskites in situ and can also be used to characterize other conductive materials of interest.

METHODS

The details of sample preparation, THz TF-TIR spectroscopy setups and measurements, XRD and PL measurements can be found in Supplemental information. The thickness of the perovskite samples was about 300 nm. The absorbance spectrum A of the sample is calculated from:

$$A = -2\log_{10}\left|\frac{FFT(T_{sample}(t)\times f(t))}{FFT(T_{reference}(t)\times f(t))}\right|, \qquad (2)$$

where $T_{sample}(t)$ and $T_{reference}(t)$ are the measured THz transmission time-domain signals of the sample and the bare substrate respectively, and $FFT()$ denotes the Fourier transform. The filter function $f(t)$ removed small reflections caused by the substrate and prism interface (contact was imperfect). Similarly, we define the logarithmic reflectance $R_{\log}$ to process the THz TF-TIR time-domain signals $R(t)$ using:

$$R_{\log} = -2\log_{10}\left|\frac{FFT(R_{sample}(t)\times f(t))}{FFT(R_{reference}(t)\times f(t))}\right|. \qquad (3)$$

The measured A and R_{log} are plotted in Figure (1) for comparison. R_{log} is fitted by LOM to extract the oscillator strength and resonant frequency. Differently from ordinary ATR, the total reflection happens at the upper surface of the sample, and thus in TF-TIR there is no restriction on the refractive index of the sample. The effects of the CYTOP encapsulation layer can be ignored, the detailed calculated results are given in the Supplemental Figure S6.

A Lorentz oscillator model (LOM) was used to fit the R_{log} spectra directly, in the form shown below[33]:

$$R_{\log} = \sum_{i=1}^{N}\frac{A_i}{(2\pi f_{0i})^2 - (2\pi f)^2 - j2\pi f\gamma_i} - A_{off} \qquad (4)$$

where f_{0i} is the resonant frequency of the ith resonance, A_i is the strength of the ith resonance and γ_i gives the information of spectral width. A_{off} is a constant offset. N is the number of the resonances, and here we choose N=2 [16, 22] but only look at the first peak considering the spectral limitation of our TIR system. We fit the spectra in the range of 0.4-

1.6 THz. Physically, in LOM fits to the permittivity of materials, A_i is positively correlated with the bound electron density of the *i*th resonance and γ_i is the phonon scattering rate[33].

ACKNOWLEDGMENT

The authors would like to thank the research grants council of Hong Kong (Project number 14201415), The Hong Kong Innovation and Technology fund (ITS/371/16), the Hong Kong PhD Fellowship award (Qiushuo Sun) and the Royal Society Wolfson Award (Emma Pickwell-MacPherson) for partial support of this work.

SUPPORTING INFORMATION

THz transmission spectra before and after illumination, PL spectra before and after illumination, THz TF-TIR spectra of the glass-encapsulated perovskite before and after illumination, XRD patterns of the encapsulated $MAPbI_2Br_1$ before and after illumination, THz TF-TIR spectra, visual images and XRD patterns of the perovskites in the presence of moisture, Calculated CYTOP effect on the THz spectra, sample preparation, THz TF-TIR spectroscopy setups and measurements, Lorentz oscillator model fitting, XRD and PL measurements (PDF).

REFERENCES

1. Correa-Baena, J.-P.; Saliba, M.; Buonassisi, T.; Grätzel, M.; Abate, A.; Tress, W.; Hagfeldt, A., Promises and challenges of perovskite solar cells. *Science* **2017,** *358* (6364), 739-744.
2. Mehmood, U.; Al-Ahmed, A.; Afzaal, M.; Al-Sulaiman, F. A.; Daud, M., Recent progress and remaining challenges in organometallic halides based perovskite solar cells. *Renewable and Sustainable Energy Reviews* **2017,** *78*, 1-14.
3. Kim, M.; Kim, G.-H.; Oh, K. S.; Jo, Y.; Yoon, H.; Kim, K.-H.; Lee, H.; Kim, J. Y.; Kim, D. S., High-Temperature–Short-Time Annealing Process for High-Performance Large-Area Perovskite Solar Cells. *ACS nano* **2017,** *11* (6), 6057-6064.
4. Xiao, Z.; Kerner, R. A.; Zhao, L.; Tran, N. L.; Lee, K. M.; Koh, T.-W.; Scholes, G. D.; Rand, B. P., Efficient perovskite light-emitting diodes featuring nanometre-sized crystallites. *Nature Photonics* **2017,** *11* (2), 108.
5. Zhu, H.; Fu, Y.; Meng, F.; Wu, X.; Gong, Z.; Ding, Q.; Gustafsson, M. V.; Trinh, M. T.; Jin, S.; Zhu, X., Lead halide perovskite nanowire lasers with low lasing thresholds and high quality factors. *Nature materials* **2015,** *14* (6), 636.
6. Gottesman, R.; Haltzi, E.; Gouda, L.; Tirosh, S.; Bouhadana, Y.; Zaban, A.; Mosconi, E.; De Angelis, F., Extremely Slow Photoconductivity Response of CH3NH3PbI3 Perovskites Suggesting Structural Changes under Working Conditions. *The journal of physical chemistry letters* **2014,** *5* (15), 2662-9.
7. Juarez-Perez, E. J.; Sanchez, R. S.; Badia, L.; Garcia-Belmonte, G.; Kang, Y. S.; Mora-Sero, I.; Bisquert, J., Photoinduced giant dielectric constant in lead halide perovskite solar cells. *The journal of physical chemistry letters* **2014,** *5* (13), 2390-2394.
8. Gottesman, R.; Gouda, L.; Kalanoor, B. S.; Haltzi, E.; Tirosh, S.; Rosh-Hodesh, E.; Tischler, Y.; Zaban, A.; Quarti, C.; Mosconi, E., Photoinduced reversible structural transformations in free-standing CH3NH3PbI3 perovskite films. *The journal of physical chemistry letters* **2015,** *6* (12), 2332-2338.
9. Nie, W.; Blancon, J. C.; Neukirch, A. J.; Appavoo, K.; Tsai, H.; Chhowalla, M.; Alam, M. A.; Sfeir, M. Y.; Katan, C.; Even, J.; Tretiak, S.; Crochet, J. J.; Gupta, G.; Mohite, A. D., Light-activated photocurrent degradation and self-healing in perovskite solar cells. *Nature communications* **2016,** *7*, 11574.
10. Noh, J. H.; Im, S. H.; Heo, J. H.; Mandal, T. N.; Seok, S. I., Chemical management for colorful, efficient, and stable inorganic–organic hybrid nanostructured solar cells. *Nano letters* **2013,** *13* (4), 1764-1769.
11. Hoke, E. T.; Slotcavage, D. J.; Dohner, E. R.; Bowring, A. R.; Karunadasa, H. I.; McGehee, M. D., Reversible photo-induced trap formation in mixed-halide hybrid perovskites for photovoltaics. *Chemical Science* **2015,** *6* (1), 613-617.
12. Slotcavage, D. J.; Karunadasa, H. I.; McGehee, M. D., Light-Induced Phase Segregation in Halide-Perovskite Absorbers. *ACS Energy Letters* **2016,** *1* (6), 1199-1205.
13. Leguy, A. M.; Goñi, A. R.; Frost, J. M.; Skelton, J.; Brivio, F.; Rodríguez-Martínez, X.; Weber, O. J.; Pallipurath, A.; Alonso, M. I.; Campoy-Quiles, M., Dynamic disorder, phonon lifetimes, and the assignment of modes to the vibrational spectra of methylammonium lead halide perovskites. *Physical Chemistry Chemical Physics* **2016,** *18* (39), 27051-27066.
14. Quarti, C.; Grancini, G.; Mosconi, E.; Bruno, P.; Ball, J. M.; Lee, M. M.; Snaith, H. J.; Petrozza, A.; Angelis, F. D., The Raman Spectrum of the CH3NH3PbI3 Hybrid Perovskite: Interplay of Theory and Experiment. *The journal of physical chemistry letters* **2014,** *5* (2), 279-84.

15. Bi, D.; Yi, C.; Luo, J.; Décoppet, J.-D.; Zhang, F.; Zakeeruddin, S. M.; Li, X.; Hagfeldt, A.; Grätzel, M., Polymer-templated nucleation and crystal growth of perovskite films for solar cells with efficiency greater than 21%. *Nature Energy* **2016,** *1* (10), 16142.
16. La-o-Vorakiat, C.; Xia, H.; Kadro, J.; Salim, T.; Zhao, D.; Ahmed, T.; Lam, Y. M.; Zhu, J. X.; Marcus, R. A.; Michel-Beyerle, M. E.; Chia, E. E., Phonon Mode Transformation Across the Orthohombic-Tetragonal Phase Transition in a Lead Iodide Perovskite CH3NH3PbI3: A Terahertz Time-Domain Spectroscopy Approach. *The journal of physical chemistry letters* **2016,** *7* (1), 1-6.
17. Milot, R. L.; Eperon, G. E.; Snaith, H. J.; Johnston, M. B.; Herz, L. M., Temperature-Dependent Charge-Carrier Dynamics in CH3NH3PbI3Perovskite Thin Films. *Advanced Functional Materials* **2015,** *25* (39), 6218-6227.
18. Park, S. J.; Kim, A. R.; Hong, J. T.; Park, J. Y.; Lee, S.; Ahn, Y. H., Crystallization Kinetics of Lead Halide Perovskite Film Monitored by In Situ Terahertz Spectroscopy. *The journal of physical chemistry letters* **2017,** *8* (2), 401-406.
19. Liu, X.; Parrott, E. P.; Ung, B. S.-Y.; Pickwell-MacPherson, E., Exploiting total internal reflection geometry for efficient optical modulation of terahertz light. *APL Photonics* **2016,** *1* (7), 076103.
20. Liu, X.; Chen, Z.; Parrott, E. P.; Ung, B. S. Y.; Xu, J.; Pickwell‐MacPherson, E., Graphene Based Terahertz Light Modulator in Total Internal Reflection Geometry. *Advanced Optical Materials* **2017,** *5* (3).
21. Harada, Y.; Ukhtary, M. S.; Wang, M.; Srinivasan, S. K.; Hasdeo, E. H.; Nugraha, A. R.; Noe, G. T.; Sakai, Y.; Vajtai, R.; Ajayan, P. M., Giant Terahertz-Wave Absorption by Monolayer Graphene in a Total Internal Reflection Geometry. *ACS Photonics* **2016**.
22. Wehrenfennig, C.; Liu, M.; Snaith, H. J.; Johnston, M. B.; Herz, L. M., Charge-carrier dynamics in vapour-deposited films of the organolead halide perovskite CH3NH3PbI3−xClx. *Energy Environ. Sci.* **2014,** *7* (7), 2269-2275.
23. Zhao, D.; Skelton, J. M.; Hu, H.; La-o-vorakiat, C.; Zhu, J.-X.; Marcus, R. A.; Michel-Beyerle, M.-E.; Lam, Y. M.; Walsh, A.; Chia, E. E., Low-frequency optical phonon modes and carrier mobility in the halide perovskite CH3NH3PbBr3 using terahertz time-domain spectroscopy. *Applied Physics Letters* **2017,** *111* (20), 201903.
24. Harwell, J. R.; Whitworth, G. L.; Turnbull, G. A.; Samuel, I. D. W., Green Perovskite Distributed Feedback Lasers. *Scientific reports* **2017,** *7* (1), 11727.
25. Nandal, V.; Nair, P. R., Predictive modeling of ion migration induced degradation in perovskite solar cells. *ACS nano* **2017,** *11* (11), 11505-11512.
26. Yuan, Y.; Huang, J., Ion Migration in Organometal Trihalide Perovskite and Its Impact on Photovoltaic Efficiency and Stability. *Accounts of chemical research* **2016,** *49* (2), 286-93.
27. Li, Z.; Lam, W.; Yang, C.; Xu, B.; Ni, G.; Abbah, S.; Cheung, K.; Luk, K.; Lu, W., Chemical composition, crystal size and lattice structural changes after incorporation of strontium into biomimetic apatite. *Biomaterials* **2007,** *28* (7), 1452-1460.
28. Niu, G.; Guo, X.; Wang, L., Review of recent progress in chemical stability of perovskite solar cells. *Journal of Materials Chemistry A* **2015,** *3* (17), 8970-8980.
29. Misra, R. K.; Aharon, S.; Li, B.; Mogilyansky, D.; Visoly-Fisher, I.; Etgar, L.; Katz, E. A., Temperature- and Component-Dependent Degradation of Perovskite Photovoltaic Materials under Concentrated Sunlight. *The journal of physical chemistry letters* **2015,** *6* (3), 326-30.
30. Buin, A.; Pietsch, P.; Xu, J.; Voznyy, O.; Ip, A. H.; Comin, R.; Sargent, E. H., Materials processing routes to trap-free halide perovskites. *Nano letters* **2014,** *14* (11), 6281-6286.

31. Noh, J. H.; Im, S. H.; Heo, J. H.; Mandal, T. N.; Seok, S. I., Chemical management for colorful, efficient, and stable inorganic-organic hybrid nanostructured solar cells. *Nano letters* **2013,** *13* (4), 1764-9.
32. Herz, L. M., Charge-carrier mobilities in metal halide perovskites: Fundamental mechanisms and limits. *ACS Energy Letters* **2017,** *2* (7), 1539-1548.
33. Parrott, E. P.; Zeitler, J. A.; McGregor, J.; Oei, S.-P.; Unalan, H. E.; Tan, S.-C.; Milne, W. I.; Tessonnier, J.-P.; Schlögl, R.; Gladden, L. F., Understanding the dielectric properties of heat-treated carbon nanofibers at terahertz frequencies: a new perspective on the catalytic activity of structured carbonaceous materials. *The Journal of Physical Chemistry C* **2009,** *113* (24), 10554-10559.